European Congress on Computational Methods in Applied Sciences and Engineering
ECCOMAS 2004
P. Neittaanmäki, T. Rossi, S. Korotov, E. Oñate, J. Périaux, and D. Knörzer (eds.)
Jyväskylä, 24–28 July 2004

# LONG-TERM BEHAVIOR OF THE WIND STRESS CIRCULATION OF A NUMERICAL NORTH ATLANTIC OCEAN CIRCULATION MODEL

**Rodolfo Bermejo Bermejo⋆, Pedro Galán del Sastre†**

⋆Universidad Politécnica de Madrid.
Escuela Técnica Superior de Ingenieros Industriales. Departamento de Matemática Aplicada.
C/ José Gutiérrez Abascal 2, 28006 Madrid, Spain
e-mail: rbermejo@etsii.upm.es

† Universidad de Castilla-La Mancha
Departamento de Matemáticas. Facultad de Ciencias del Medio Ambiente.
Avda. Carlos III s/n, 45074 Toledo, Spain
e-mail: pedro.galan@uclm.es

**Key words:** wind-driven, barotropic ocean circulation, numerical modeling, POD.

**Abstract.** *We present a numerical study of long-term calculation of a barotropic North-Atlantic Ocean circulation model. The aim of the paper is twofold. First, we present an efficient semi-Lagrangian projection scheme for an eddy resolving circulation model and second, we use the so called proper orthonormal decomposition technique to calculate a finite dimensional subspace that contains the dynamics of the solution. Using a Galerkin projection on this subspace, we reduce the high dimensional system, obtained by the application of the finite element method to discretize in space the equations of the model, to a low dimensional system and, thus, we can calculate the bifurcation diagram using the software of AUTO having as a control parameter the horizontal eddy viscosity coefficient.*

## 1 Introduction

On a large scale, the ocean circulation system is driven by wind-stress, heat and fresh water fluxes. The wind-stress is the main driving mechanism to the circulation of the ocean upper layer, which is the water layer between the sea surface and a depth of about few hundred meters, this circulation is also known as ocean surface circulation; whereas heat and fresh water fluxes are responsible of the thermohaline circulation, which is the component of the ocean circulation system with time scales ranging from decades to centuries and spatial scales extending over the whole ocean basin, so that, the thermohaline circulation has a strong influence on the long time scales of climate variability. The surface circulation determines the sea surface temperature and is involved in short time scales of climate variability. The main feature of the wind driven circulation at mid-latitudes is the presence of a double gyre phenomenon with a strong boundary current at the lower gyre, such boundary current extends as a jet to the interior of the ocean. These gyres have a typical horizontal scale of about one thousand kilometers and are persistent and dominant. They represent the seasonal and inter-annual variability of large scale ocean surface circulation at mid-latitudes, and they also transfer potential energy.

Wind-driven circulation is basically a non-linear phenomenon and as such, there have been many authors who have studied it. Thus, Veronis (1963) was the first to analyze multiple steady states and transition to periodic solutions in the lower gyre. Bryan (1963) was the first to apply a numerical formulation to study the time dependent solution of a barotropic quasi-geostrophic ocean driven by steady wind stress. More recently, Jiang (1995) calculates a bifurcation diagram for a wind-driven double gyre shallow water model as a control parameter takes different values. The diagram shows the transition of the ocean circulation regime from multiple steady states to periodic and aperiodic states. Berloff and Meachan (1997) study the bifurcation structure of a barotropic wind-driven model for a small mid-latitude ocean basin. Chang et al. (2001) trace the bifurcation diagram for a barotropic double-gyre mid-latitude quasi-geostrophic ocean and Simonet et al. (2001) have done a similar study in a shallow water model for the wind-driven ocean circulation with numerical simulations carried out for an idealized North Atlantic with a constant depth. The main goal of this article is to show the behavior of numerical solutions when long time computations are performed in a barotropic ocean including bottom topography, realistic boundaries and real climate wind stress.

## 2 The Model

The ocean model is a barotropic (constant density $\rho_0$) mid-latitude $\beta$-plane ocean domain $\Omega$ of variable depth $H$ and free surface $\overline{D} = D \cup \partial D$, which is driven by climatic wind stress acting upon the sea surface $D$. For such a model, the system of Primitive Equations that govern the general ocean dynamics [14] can be integrated in the vertical to yield the following 2D Navier-Stokes equations

$$\begin{cases} \dfrac{D(\overline{u})}{Dt} + f(\overline{u})^{\perp} + H\nabla p - \nu_h \Delta(\overline{u}) + \gamma(\overline{u}) = \tau, & in\ D \times (0,T] \\ div(\overline{u}) = 0 \end{cases} \tag{1}$$

with the following initial and boundary conditions:

$$\begin{cases} \overline{u} = 0\ in\ D \text{ for } \ t = 0 \\ \overline{u}\ |_{\partial D} = 0 \ \text{ and } \overline{u} \cdot n\ |_{(-H)} = 0 \ \ \forall t. \end{cases} \tag{2}$$

We explain now the notation used in (1) and (2). Let $u_H(x,t)$ be the horizontal velocity vector in the Primitive Equations which satisfies

$$div \int_{-H}^{0} u_H dz = 0 \text{ in } \Omega \times [0,T],$$

and on the solid boundaries $\Gamma_s$of $\Omega$

$$u_H\ |_{\Gamma_s} = 0,$$

where $\Gamma_s$ is composed by the lateral boundaries $\Gamma_l$ and the bottom topography $H(x,y),\ H \geq H_0$, with $H_0 > 0$ being a constant , we define the vector $\overline{u}$ as

$$\overline{u} = \int_{-H}^{0} u_H dz. \tag{3}$$

In (2) $n$ denotes the unitary outward normal vector. The function $f$, known as the Coriolis parameter, represents the planetary vorticity of the motion due to the rotation of the Earth. The mathematical expression for $f$, assuming that the Earth is a perfect sphere, is

$$f = 2\Omega \cos\theta,$$

where $\Omega = 7.2526 \times 10^{-5} s^{-1}$ denotes the angular velocity of the Earth and $\theta$ $(0 \leq \theta \leq \pi)$ is the colatitude. The $\beta$-plane approximation (see [17] for a physical justification and mathematical details) consists of projecting the spherical surface on its tangent plane at a mid-latitude point $(\psi_0, \theta_0) \in D$, and defining on such a plane a local Cartesian coordinate system $(x,y)$ with origin at $(\phi_0, \theta_0)$ such that

$$x_1 := \frac{\phi - \phi_0}{a} \ \text{ and } \ x_2 := \frac{\theta - \theta_0}{a},$$

where $a$ is the radius of the Earth and the coordinates $(x,y)$ being positive in the east and north directions, respectively. In doing so, one approximates the true value of the Coriolis parameter $f$ by its linear approximation about the origin as

$$f = f_0 + \beta x_2 \tag{4}$$

where

$$f_0 = 2\Omega \cos\theta_0 \quad \text{and} \quad \beta = \frac{1}{a}\frac{df}{d\theta} \mid_{\theta=\theta_0} \tag{5}$$

So that, the Primitive Equations formulated in spherical coordinates are approximated by the formulation in the local Cartesian coordinates of the tangent plane. It is considered that this methodology of simplifying the Primitive Equations is a first order approximation for studying the large scale ocean dynamics, which is only valid at mid-latitudes, say, $20^o \leq \theta \leq 50^o$.

The total derivative is then given by

$$\frac{D(\overline{u})}{Dt} = \frac{\partial(\overline{u})}{\partial t} + (\frac{\overline{u}}{H} \cdot \nabla)(\overline{u}) \tag{6}$$

The external forcing terms are represented by the steady wind stress $\boldsymbol{\tau}(x) = (\tau_1(x_1, x_2), \tau_2(x_1, x_2))$. $\nu_h$ is a constant horizontal eddy viscosity coefficient and $\gamma$ is a constant bottom friction coefficient.

The model (1)-(2) is dynamically equivalent to the barotropic streamfunction-vorticity model used by Munk (1950) and Munk and Carrier (1950) to understand the role that both the horizontal dissipation and Coriolis force play in the westward intensification of the wind driven ocean circulation. The same model, but with the non linear terms, was used by Bryan (1963) to carry out one of the early numerical simulations of the ocean circulation. One can prove existence and uniqueness for the weak solution to (1) and (2) in the subspaces $H_1$ and $V_1$ defined as follows

$$\begin{gathered} \mathcal{D}(D) = \{\varphi \in C_0^\infty(D\}, \\ \mathcal{V}_1(D) = \{v \in \mathcal{D}(D)^2 : divv = 0 \text{ and } v \cdot \nabla H = 0\} \\ H_1 = \overline{\mathcal{V}_1(D)}^{L^2(D)^2} \text{ and } V_1 = \overline{\mathcal{V}_1(D)}^{H_0^1(D)^2}. \end{gathered} \tag{7}$$

From a mathematical point of view it seems to be restrictive seeking a solution in the subspace $V_1$. One can remove such a restriction by reformulating the way the viscous terms are derived in (1). Defining the vertically averaged velocity vector

$$u = \frac{\overline{u}}{H}, \tag{8}$$

we obtain the following equations for the barotropic ocean model

$$\begin{cases} H\dfrac{Du}{Dt} + fHu^\perp + H\nabla p - div(\nu_h H\nabla(u)) + \gamma Hu = \tau, \ \ in\ D \times (0,T] \\ div(Hu) = 0 \end{cases} \tag{9}$$

subjected to the initial and boundary conditions

$$\begin{cases} u = 0\ in\ D \text{ for } \ t = 0 \\ u \mid_{\partial D} = 0 \ \text{ and } u \cdot n \mid_{(-H)} = 0 \ \ \forall t. \end{cases} \tag{10}$$

In (9) the total derivative is given by

$$\frac{Du}{Dt} = \frac{\partial u}{\partial t} + u \cdot \nabla u. \tag{11}$$

We end this section by establishing the existence and uniqueness of the solution $(u, p)$ to (9)-(10) in the spaces

$$\begin{array}{c} \mathcal{V}(D) = \{ v \in \mathcal{D}(D)^2 : div Hv = 0 \ \} \\ H = \overline{\mathcal{V}(D)}^{L^2(D)^2} \text{ and } V = \overline{\mathcal{V}(D)}^{H_0^1(D)^2} \end{array} \tag{12}$$

and defining the bilinear form

$$\begin{array}{c} a : H_0^1(D)^2 \times H_0^1(D)^2 \to \mathbf{R} \\ a(u, v) = \gamma(Hu, v) + \nu_h(H\nabla u, \nabla v) \end{array} \tag{13}$$

where $(\cdot, \cdot)$ denotes the $L^2$ inner product, and the trilinear form

$$\begin{array}{c} d : H_0^1(D)^2 \times H_0^1(D)^2 \times H_0^1(D)^2 \to \mathbf{R} \\ d(u, v, w) = \int_D (Hu \cdot \nabla v) \cdot w dx. \end{array} \tag{14}$$

It is easy to show the following properties: (i) $a(u, v)$ is a continuous and coercive bilinear form; (ii) $d(u, v, w) = -d(u, w, v)$, this property implies that $d(u, v, v) = 0$ and (iii) there exists a constant $C$ such that $\mid d(u, u, v) \mid \leq C \parallel u \parallel_{L^2(D)^2} \parallel u \parallel_{H_0^1(D)^2} \parallel v \parallel_{H_0^1(D)^2}$ . See [19] for other well known inequalities satisfied by $\mid d(u, u, v) \mid$ We are now in a condition to define the weak solution to problem (9)-(10).

**Definition 1.** *A weak solution to equations (9) and (10) is a function* $u \in L^2(0, T; V) \cap L^\infty(0, T; H)$ *satisfying* $u_t \in L^2(0, T; V')$ *and*

$$\langle Hu_t, v \rangle + (fHu^\perp, v) + d(u, u, v) + a(u, v) = (\tau, v) \ \ \forall v \in V.$$

We establishes without proof the existence and uniqueness of the weak solution [9].

**Theorem 1(Weak solution).** *If* $\tau \in L^2(D)$ *the weak solution* $u$ *is unique and* $u \in C(0, T; H)$.

## 3 The numerical method

To compute the approximate solution to (9)-(10) we discretize in time and space the velocity and pressure. For space discretization we use the finite element method because of its good properties to deal with the irregular shape of the ocean coastlines and its flexibility to make local mesh refinements. As for time discretization we choose a semi-Lagrangian projection scheme.

### 3.1 Finite element approximation: generalities

Given the real parameter $h_0,\ 0 < h_0 < 1$, let $h$ be a space discretization parameter such that $0 < h < h_0$. To compute a numerical solution of (9) and (10) we generate a quasi-uniform partition $D_h$ in $\overline{D}$ composed of elements $T_j$ with Lipschitz boundary $\Gamma_j$ that satisfy the following conditions: (i) Let $NE$ be the number of elements in $D_h$, then $\overline{D} = \bigcup_j \overline{T}_j,\ j = 1, .., NE$. (ii) For $1 \leq j, l \leq NE,\ j \neq l$,

$$\overline{T}_j \cap \overline{T}_l = \begin{cases} P_i,\ a\ mesh\ point,\ or \\ \Gamma_{jl},\ a\ common\ side,\ or \\ \emptyset,\ empty\ set\ otherwiae. \end{cases}$$

(iii) There is a positive constant $\mu$ such that for all $T_j,\ \dfrac{d_j}{h_j} > \mu$, where $d_j$ denotes the diameter of the circle inscribed in $T_j$ and $h_j$ is the diameter of $T_j$, such that $h = \max_j h_j$. Next, we associate a family of finite element spaces with the partition $D_h$. To do so, we consider an element of reference $\widehat{T} \subset \mathbf{R}^2$ such that for each element $T_j$ of $D_h$ we can define a one-to-one mapping $F_j : \widehat{T} \to T_j$ such that if $\widehat{P}_m(\widehat{T})$ is the set of polynomials $\widehat{p}(\widehat{x})$ of degree $\leq m$ defined on $\widehat{T}$, then for each $T_j$ there exists a set

$$P_m(T_j) = \{p(x), x \in T_j(x) : p(x) = \widehat{p}(F_j^{-1}(x))\}.$$

We now define the family of conforming finite element spaces

$$\begin{gathered} V_h = \{v_h \in (C^0(\overline{D}))^d : v_h \mid_{T_j} \in P_2(T_j), 1 \leq j \leq NE\} \\ Q_h = \{q_h \in C^0(\overline{D}) : q_h \mid_{T_j} \in P_1(T_j), 1 \leq j \leq NE\} \\ V_{h0} = \{v_h \in V_h : v_h \mid_{\partial D_1} = 0\}. \end{gathered} \tag{15}$$

We also consider the space

$$S_h = Q_h \cap L_0^2, \tag{16}$$

where

$$L_0^2 = \{q \in L^2(D) : \int_D q ds = 0\}. \tag{17}$$

The finite element spaces have the following approximation properties.

*A1) (Inf-sup) There exists a positive constant $\beta$ independent of $h$ tal que*

$$\inf_{q_h \in Q_h} \sup_{u_h \in V_h} \frac{b(u_h, q_h)}{\parallel u_h \parallel_1} \geq \beta \parallel q_h \parallel,$$

where the bilinear form $b : V_{h0} \times Q_h \to \mathbf{R}$ is defined by

$$b(u_h, q_h) = -\int_D q_h div(H u_h) dx. \tag{18}$$

*A2) For all* $u \in H^{r+1}(D)$, $q \in H^r(D)/R$, $1 \leq r \leq m$, *there exist positive constants* $K$ *such that*

$$\inf_{u_h \in V_h} \{\| u - u_h \| + h \| u - u_h \|_1 \leq K h^{m+1} \| u \|_{m+1},$$

and

$$\inf_{q_h \in Q_h} \| q - q_h \| \leq K h^r \| q \|_{H^r/\mathbf{R}} .$$

Let MV and MP the number of nodes in the velocity and pressure meshes respectively, then $v_h \in V_h$ and $q_h \in Q_h$ are expressed as

$$\begin{aligned} v_h &= \textstyle\sum_{k=1}^{MV} V_k \phi_k, \\ q_h &= \textstyle\sum_{l=1}^{MP} Q_l \psi_l, \end{aligned} \tag{19}$$

where $\{\phi_k\}_{k=1}^{MV}$ $\{\psi_l\}_{l=1}^{MP}$ denote the global basis of $V_h$ and $Q_h$ respectively. The functions $\phi_k$ and $\psi_l$ are characterized by satisfying $\phi_k(x_j) = \delta_{kj}$ and $\psi_l(y_i) = \delta_{ki}$; $\{y_i\}_{i=1}^{MP}$ and $\{x_j\}_{j=1}^{MV}$ being the sets of nodes for pressure and velocity respectively in the partition $\bar{D}_h$. Before proceeding to the description of the semi-Lagrangian projection scheme we write the formulation of the semi-discrete finite element solution to problem (9)-(10). To this end, we shall consider the restriction of the bilinear form $a$ and the trilinear form $d$ onto the finite element space $V_{h0} \subset H_0^1$. Thus, for $(u_h, v_h) \in V_{h0} \times V_{h0}$

$$a(u_h, v_h) = \gamma(H u_h, v_h) + \nu_h(H \nabla u_h, \nabla v_h) \tag{20}$$

This bilinear form defines a discrete operator $A_h : V_{h0} \to V_{h0}$ such that for all $v_h \in V_{h0}$

$$A_h u_h, v_h) = a(u_h, v_h). \tag{21}$$

Similarly, we associate with the bilinear form $b$ the operator $B_h : V_{h0} \to Q_h$ and its transpose $B_h^t : Q_h \to V_{h0}$ defined as

$$(B_h u_h, q_h) = b(u_h, q_h) = (B_h^t q_h, u_h), \ \forall u_h \in V_{h0} \text{ and } \forall q_h \in Q_{h.} \tag{22}$$

We also need the bilinear discrete operator $D_h(\cdot, \cdot)$ associated with the restriction of the trilinear form $d$ onto $V_{h0}$, the discrete Coriolis operator $C_h$ and the orthogonal projector $P_h$ onto $V_{h0}$. Thus, for any $w_h \in V_{h0}$

$$\begin{gathered} D_h : V_{h0} \times V_{h0} \to V_{h0} \\ (D_h(u_h, v_h), w_h) = d(u_h, v_h, w_h) \end{gathered} \tag{23}$$

$$(C_h u_h, w_h) = (H f u_h^{\perp}, w_h) \tag{24}$$

and

$$\begin{gathered} P_h : L^2(D) \to V_{h0} \\ (P_h v, w_h) = (v, w_h) \end{gathered} \tag{25}$$

Note that $d(u_h, v_h, w_h) = -d(u_h, w_h, v_h)$ and $d(u_h, v_h, v_h) = 0$. Also, it is worth noticing that $(C_u u_h, u_h) = 0$. We are now in a position to formulate the semi-discrete approximate solution $(u_h(t), p_h(t))$ to problem (9)-(10). Find $u_h : (0, T] \to V_{h0}$ and $p_h : (0, T] \to Q_h$ such that

$$\begin{array}{c} H\dfrac{Du_h}{Dt} + A_h u_h + C_h u_h + B_h^t p_h = P_h \tau \\ B_h u_h = 0 \\ u_h(0) = 0. \end{array} \tag{26}$$

Here, $H\dfrac{Du_h}{Dt} = H\dfrac{\partial u_h}{\partial t} + D_h(u_h, u_h)$ is an approximation in $V_h$ to the total derivative operator $H\dfrac{Du}{Dt}$.

### 3.2 The semi-Lagrangian projection scheme

There are several difficulties to compute a numerical solution to (9)-(10), being the most relevant the following ones: (i) the nonlinearity of the model represented by the term $u \cdot \nabla u$; (ii) the incompressibility condition or equivalently, the condition $div(Hu) = 0$, and (iii) the Coriolis term that can cause instabilities when the viscous terms are small. To be efficient, we have chosen a pressure-correction projection scheme implemented in a semi-Lagrangian framework. Thus, let $I_N := \{t_0, t_1, .., t_N\}$ be a uniform partition of the interval $[0, T]$ with step-length $\Delta t$. A fully discrete approximate solution to (9) and (10) is the pair of mappings $u_h : I_n \to V_{h0}$ and $p_h : I_N \to Q_h$ such that for $n = 1, 2, ...$

$$u_h^n = \sum_{k=1}^{MV} U_k^n \phi_k \tag{27}$$

and

$$p_h^n = \sum_{j=1}^{MP} P_j^n \psi_k. \tag{28}$$

The semi-Lagrangian pressure-correction projection scheme combines a semi-Lagrangian method to discretize the total derivative operator, with a pressure-correction scheme [11] that calculates the solution $(u_h^{n+1}, p_h^{n+1})$ in a two step procedure. In the first one, an intermediate velocity $\widetilde{u}_h^{n+1}$ is calculated by solving a Burger´s problem, so that, $\widetilde{u}_h^{n+1}$ is not divergence free but it satisfies the boundary condition, this implies that $\widetilde{u}_h^{n+1} \in V_{h0}$; in the second step, $(u_h^{n+1}, p_h^{n+1})$ are calculated, now $u_h^{n+1}$ is divergence free but it does not satisfy the boundary conditions, so that $u_h^{n+1} \notin V_{h0}$. The semi-Lagrangian scheme is applied in the first step to discretize the total derivative operator along its characteristic curves $X(x, s; t)$. If the velocity vector $u(x, t)$ is Lipschitz continuous then $X\ (x, s, t)$ is the unique solution to the differential equation

$$\begin{array}{c} \dfrac{dX}{d\tau} = u(X(x, s; \tau), \tau) \\ X(x, s; s) = x \end{array}$$

or equivalently, for $\tau$ in the interval $(t, s)$

$$X(x, s; t) = x - \int_t^s u(X(x, s; \tau), \tau) d\tau. \tag{29}$$

Now, setting $t = t_n$, $s = t_{n+1}$ and approximating $H\dfrac{Du_h}{Dt}$ by the second order BDF scheme (*Backward Differentiation Formulas*, Chapter III.1 in [12]) along the characteristics curves $X(x, s; t)$ we obtain that

$$H\frac{Da_h}{Dt} \mid_{t=t_{n+1}} \simeq H\frac{3a_h^{n+1} - 4\overline{a}_h^n + \overline{a}_h^{n-1}}{2\Delta t} \tag{30}$$

where $\overline{a}_h^n = a_h(X_h(x, t_{n+1}; t_n), t_n)$, $\overline{a}_h^{n-1} = a_h(X_h(x, t_{n+1}; t_{n-1}), t_{n-1})$ and $X_h(x, t_{n+1}; t_{n-1})$ denotes the approximate foot of the characteristic curve at time $t_n$, or in other words, the position at time $t_n$ of a moving point that at time $t_{n+1}$ will arrive at $x$. In the framework of the semi-Lagrangian formulation, there are many methods to compute the points $X_h(x, t_{n+1}; t_{n-1})$ as well as the functions $\overline{a}_h^n$. We describe our semi-Lagrangian scheme as follows.

(1) *The quasi-monotone semi-Lagrangian step*

Let $Y_h = V_{h0} + \nabla Q_h$. Suppose that at time $t_n$ we know the solution $(u_h^n, p_h^n) \in Y_h \times Q_h$, and the orthogonal projections $w_h^n = P_h u_h^n$ and $w_h^{n-1} = P_h u_h^{n-1} \in V_{h0}$. We calculate the values $\overline{w}_h^n$ and $\overline{w}_h^{n-1}$ as follows:

(1.1) For each velocity mesh-point $x_k$ which is not on the boundary, we compute the points $X_{hk}^{n-l} := X_h(x_k, t_{n+1}; t_{n-l})$, where the superscript $l$ takes the values 0 and 1. To do so, we set [1]

$$X_{hk}^n = x_k - \alpha_{hk}$$

and $\alpha_{hk}$ is approximated by the fixed iteration process

$$\alpha_{hk}^{(r+1)} = \frac{\Delta t}{2}\left[3w_h^n(x_k - \frac{1}{2}\alpha_{hk}^{(r)}) - w_h^{n-1}(x_k - \frac{1}{2}\alpha_{hk}^{(r)})\right]. \tag{31}$$

The values of $w_h^n(x_k - \frac{1}{2}\alpha_{hk}^{(r)})$ and $w_h^{n-1}(x_k - \frac{1}{2}\alpha_{hk}^{(r)})$ are calculated by finite element interpolation in $V_{h0}$. Analogously, we set for $l = 1$

$$X_{hk}^{n-1} = x_k - \alpha_{hk}, \tag{32}$$

now, $\alpha_{hk}$ is calculated similarly as above by the fixed point iteration

$$\alpha_{hk}^{(r+1)} = 2\Delta t\left[w_h^n(x_k - \alpha_{hk}^{(r)})\right]. \tag{33}$$

Once we know the coordinates of the feet of the Characteristics we proceed to evaluate $w_h^n$ and $w_h^{n-1}$ at these points. There are several approaches to do so, see, for instance, [8] and [18]; however, unlike these authors, who use a $L^2$ projection of $w_h^n(X_h^n)$ and $w_h^{n-1}(X_h^{n-1})$ onto $V_h$, we propose an interpolatory projection to compute the values of $w_h^n$ and $w_h^{n-1}$ at the points $X_{hk}^n$ and $X_{hk}^{n-1}$ respectively. This way of performing the method of Characteristics yields the so called semi-Lagrangian schemes. The latter are computationally more efficient than the $L^2$projection and must be used with polynomials of degree equal or larger than two in order to achieve an asymptotic error estimate of order higher than two. The problem associated to interpolation by polynomials of degree equal or larger than two is the possible generation of wiggles and consequently the loss of uniform stability of the method. To overcome this trouble, we make use of the so called quasi-monotone semi-Lagrangian scheme [4] and [3].

(1.2) Let $p(k)$ be the element of $D_h$ where $X_{hk}^{n-l}$ is located, and let $\left\{W_1^{n-l}, W_2^{n-l}, .., W_{NH}^{n-l}\right\}$ be the set of nodal values of $w_h^{n-j}$ in $p(k)$.

Calculate

(i)

$$W_k^{*n-l} = w_h^{n-l}(X_{hk}^{n-l}) = \sum_{i=1}^{NH} W_i^{n-l}\varphi_i(X_{hk}^{n-l}) \tag{34}$$

where $\{\varphi_i(x)\}_{i=1}^{NH}$ is the set of nodal basis functions for the element $p(K)$

(ii)

$$\begin{array}{l} W^{l+} := Max(W_1^{n-l}, ..., W_{NH}^{n-l})_{p(k)} \\ W^{l-} := Min(W_1^{n-l}, ..., W_{NH}^{n-l})_{p(k)} \end{array} \tag{35}$$

(iii) Set

$$\overline{W}_k^{n-l} = \left\{ \begin{array}{c} W^{l+}\ if\ W_k^{*n-l} > W^{l+}, \\ W^{l-}\ if\ W_k^{*n-l} < W^{l-}, \\ W_k^{*n-l},\ otherwise. \end{array} \right. \tag{36}$$

And finally, set

$$\overline{w}_h^{n-l} = \sum_{k=1}^{M} \overline{W}_k^{n-l}\phi_k(x). \tag{37}$$

**Remark 1** *As is shown in [3] the values $\overline{W}_k^{n-l}$ can also be expressed as*

$$\overline{W}_k^{n-l} = (1 - C_k^{n-l})I_1 W^{n-l}(X_{hk}^{n-l}) + C_k^{n-l} I_2 W^{n-l}(X_{hk}^{n-l}),$$

*where $I_s : C^0(\overline{D}) \to V_h$ is the piecewise Lagrange interpolation operator of degree $s$, and $C_k^{n-l}$ is a limiting coefficient given by*

$$C_k^{n-l} = Min\left(1, \left\{ \begin{array}{c} \dfrac{W^{l+} - I_1 W^{n-l}(X_{hk}^{n-l})}{P^{n-l}},\ \ if\ \ P^{n-l} > 0, \\ \dfrac{W^{l-} - I_1 W^{n-l}(X_{hk}^{n-l})}{P},\ \ if\ \ P^{n-l} < 0, \\ 1\ if\ \ P^{n-l} = 0 \end{array} \right.\right),$$

*with* $P^{n-l} = I_2W^{n-l}(X_{hk}^{n-l}) - I_1W^{n-l}(X_{hk}^{n-l})$. *The role of the limiting coefficient is to suppress the oscillations generated by the polynomials of degre larger or equal than two by weighting with linear polynomials which are monotone. In regions where the solution is sufficiently smooth and the oscillations are zero or very small, the limitiing coefficients take the value one or very close to one and, therefore, the numerical solution is basically that given by the polynomials of higher degree.*

*Next, we proceed to compute* $\widetilde{u}_h^{n+1} \in V_{h0}$, $u_h^{n+1} \in Y_h$ *and* $p_h^{n1} \in Q_h$ *by the projection method performing:*

*(2) The Viscous step*

$$H\frac{3\widetilde{u}_h^{n+1} - 4\overline{w}_h^n + \overline{w}_h^{n-1}}{2\Delta t} + A_h\widetilde{u}_h^{n+1} + C_h(2\overline{w}_h^n - \overline{w}_h^{n-1}) + \kappa B_h^t p_h^n = P_h\tau. \tag{38}$$

*(3) The Projection step*

$$\begin{gathered}(H\nabla(p_h^{n+1} - p_h^n), \nabla q_h) = -\frac{3}{2\Delta t}(divH\widetilde{u}_h^{n+1}, q_h) \quad \forall q_h \in Q_h,\\ u_h^{n+1} = \widetilde{u}_h^{n+1} - \Delta t\nabla(p_h^{n+1} - \kappa p_h^n),\\ (P_h u_h^{n+1}, v_h) = (u_h^{n+1}, v_h) \ \ \forall v_h \in V_{h0},\end{gathered} \tag{39}$$

where the parameter $\kappa$ takes the values 0 or 1

*(4)* Set $n = n + 1$ and go to (1)

Several remarks are now in order.

(1) The space $Y_h$ was introduced in [10] in its analysis of projection schemes. $Y_h = V_{h0} + \nabla Q_h$.

(2) Note that the first two equations in (39) define a problem equivalent to the following one: find $u_h^{n+1} \in Y_h$ such that

$$\begin{gathered}\left(\frac{3u_h^{n+1} - 3i_h\widetilde{u}_h^{n+1}}{2\Delta t}, z_h\right) + \left(H\nabla(p_h^{n+1} - p_h^n), z_h\right) = 0, \ \ \forall z_h \in Y_h\\ (divHu^{n+1}, q_h) = 0 \quad \forall q_h \in Q_h.\end{gathered}$$

(3) $u_h^{n+1} \in Y_h$ is discontinuous at the inter-element boundaries, so that we need to calculate $w_h^{n+1} = P_h u_h^{n+1}$, which is a Lipschitz continuous velocity, as the velocity to be used in the semi-Lagrangian step to compute the points $X_{hk}^{n+1}$.

## 4 Numerical experiments

We have applied the numerical scheme described above to simulate the wind driven circulation in a subdomain $D$ of the North Atlantic Ocean which extends from $15^oN$ up to $65^oN$. Figure 1 shows this domain and the isolines of the bottom topography $H(x, y)$ used

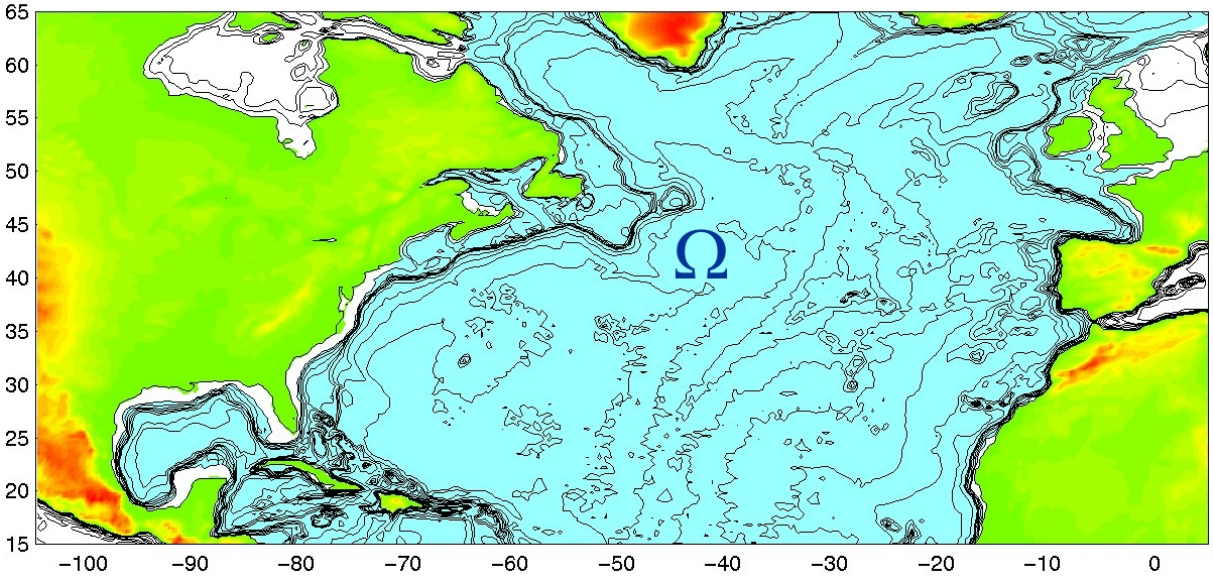


Figure 1:

in the experiments. Since the wind- driven circulation is confined in the upper layer, we have restricted the range of variation of $H(x, y)$ between $50m$ and $1000m$ for all $(x, y)$. Figure 2 (upper panel) shows the climatological wind stress pattern that forces the model. This pattern has been obtained by averaging Hellerman Rosenstein monthly wind stress data. The centre of the $\beta-$plane approximation is at $\theta_0 = 40^O N$. The computational mesh is composed of $P_2 - P_1$ elements in order to satisfy the inf-sup condition. The size of the elements of the computational mesh ranges from $10km$ in the region of The Gulf Stream up to $40Km$ in many regions of the interior of the domain where the flow is very smooth. The total number of elements is 124244 and there are 250715 velocity nodes and 63235 pressure nodes. A detail of the mesh in the region of The Gulf Stream is shown in Figure 2 (lower panel), here the elements are small because is a region where the flow undergoes strong variations. A time step $\Delta t = 2$ *hours* is used in all the numerical experiments run with the model. To better see the influence of the depth in the long term dynamics of a barotropic model, we have run a first experiment with a constant depth $H = 1000m$ and an eddy viscosity coefficient $\nu_h = 2000m^2 s^{-1}$. The model is quite dissipative and, therefore, reaches the steady state at $T = 120$ . The stream lines of the steady flow are depicted in Figure 3 (upper panel) where we can distinguish two closed circulation patterns, an anticlockwise pattern in the northern part of the domain and a clockwise pattern in the southern basin. In this circulation patterns it is noticeable the westward intensification of the flow along the North America coast. From the tip of the Florida coast up to about $40^o N$ the intensification hypothetically corresponds to The

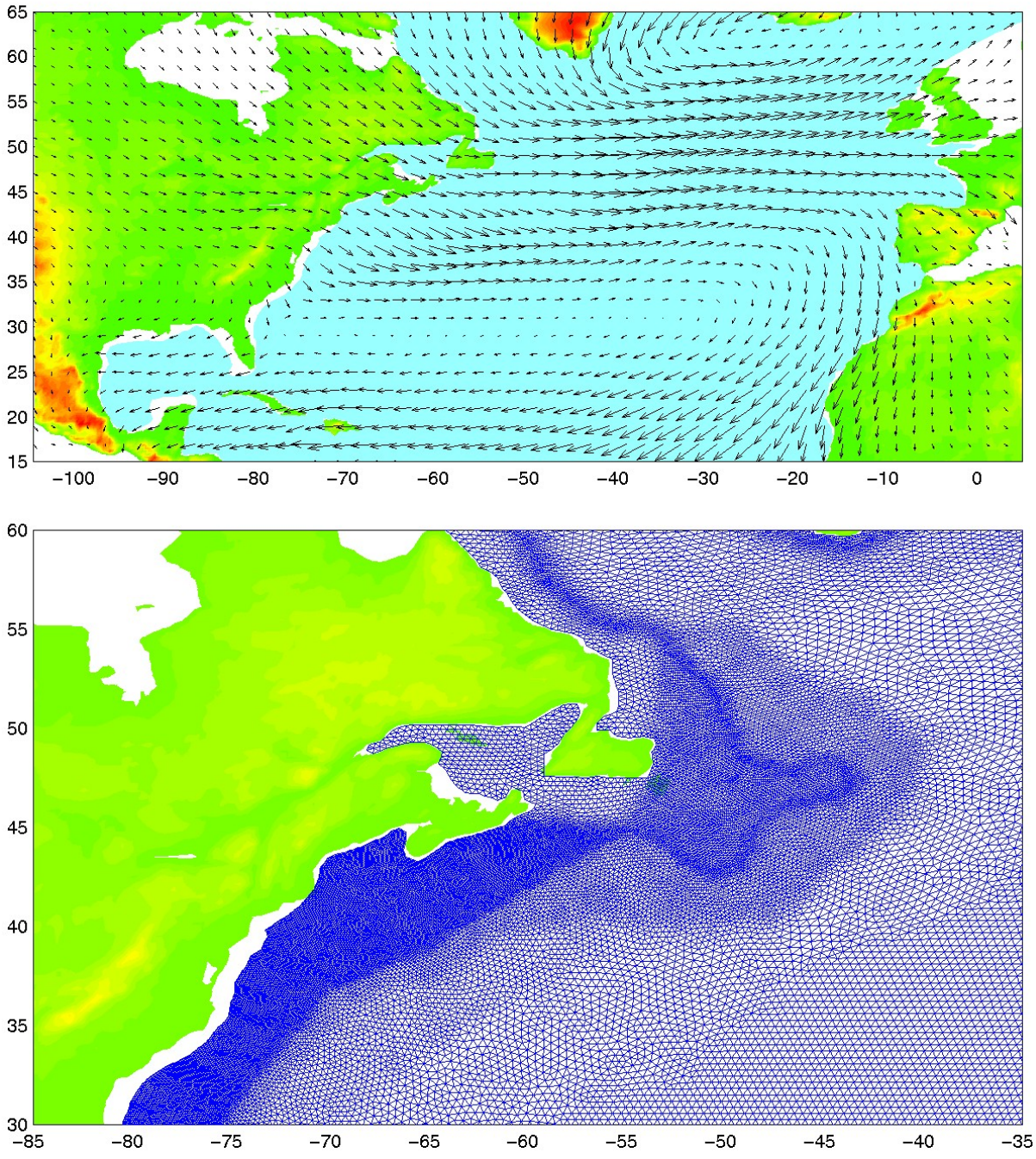
65
60
55
50
45
40
35
30
25
20
15
−100
−90
−80
−70
−60
−50
−40
−30
−20
−10
0
60
55
50
45
40
35
30
−85
−80
−75
−70
−65
−60
−55
−50
−45
−40
−35

Figure 2:

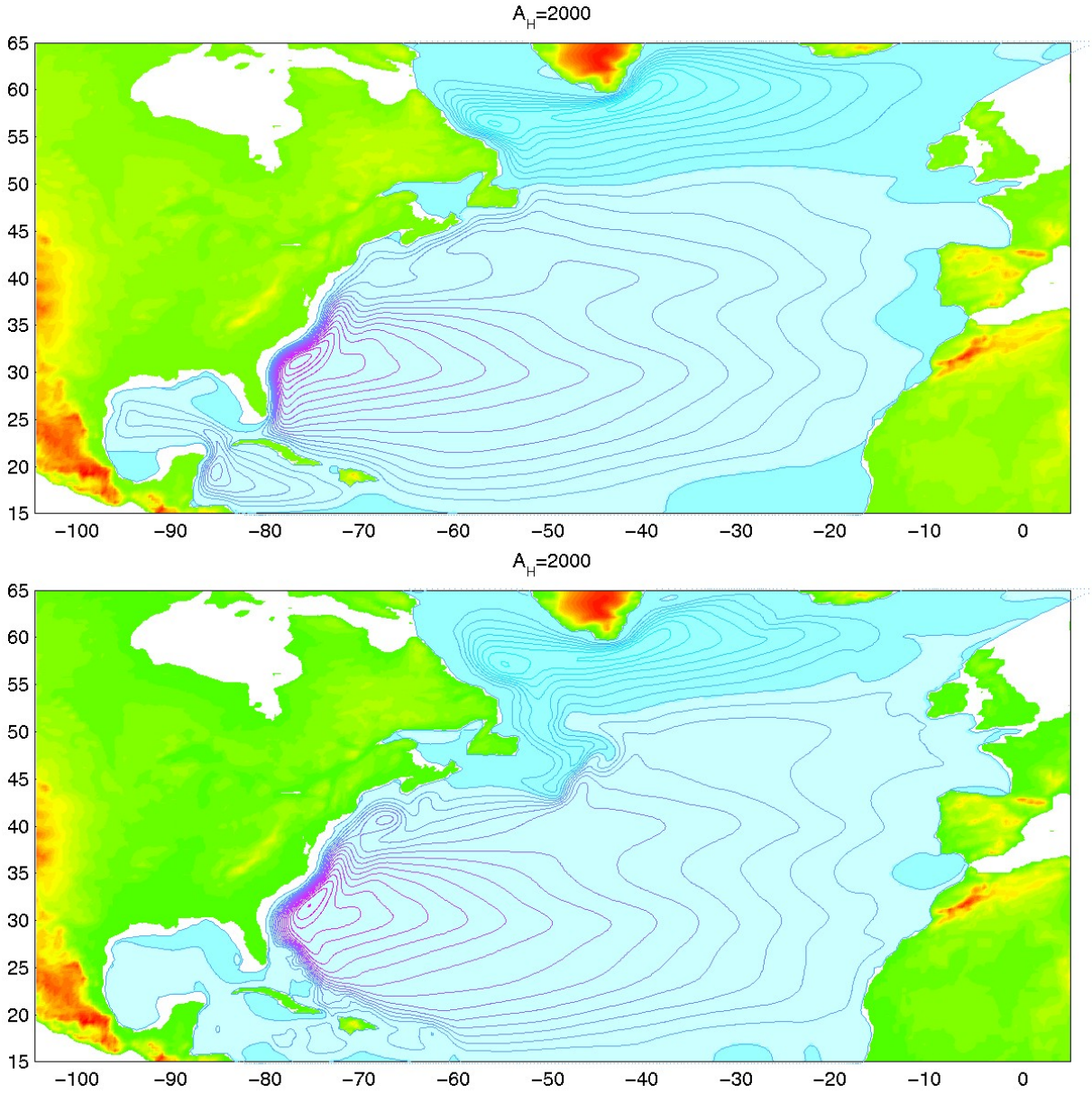


Figure 3:

Gulf Stream, whereas the intensification which appears along the Newfoundland coast corresponds to The Labrador Current. There are no interaction between the upper and lower circulation patterns. However, things are different when the experiment includes the bottom topography as Figure 3 (lower panel) shows. Here, we can see that the The Labrador Current comes further down to the South due to the fact that the presence of the George Banks prevents the lower current to penetrate further up to the North. As

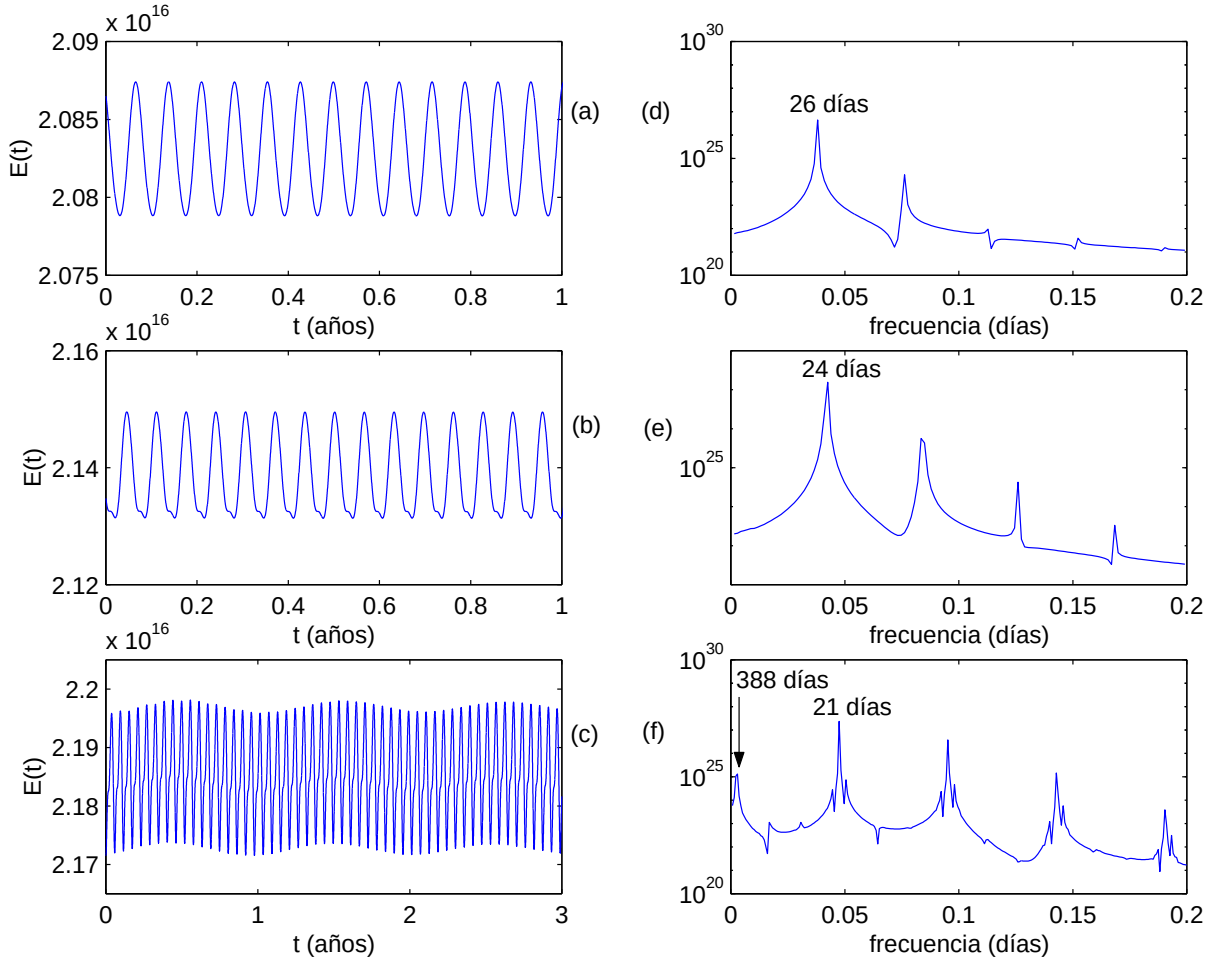


Figure 4:

the eddy viscosity coefficient $\nu_h$ is decreased the flow takes longer to reach the steady state and for $\nu_h = 670 \pm 5 m^2 s^{-1}$ the flow experiences the first Hopf bifurcation. In Figure 4 we show the time history of the energy of the flow and the corresponding spectrum for three viscosities. The flow is periodic for $\nu_h = 670 m^2 s^{-1}$ with a period of 26 days and for $\nu_h = 650 m^2 s^{-1}$ with a period of 24 days; however, for $\nu_h = 640 m^2 s^{-1}$ the flow has already undergone another bifurcation and the periodic structure has become quasi-periodic because of the presence of two rationally independent periods (or frequencies), one is 21 days and the second one is 388 days. A further reduction in the eddy viscosity $\nu_h$ produces a-periodic states. Figure 5 shows a sequence of aperiodic states of the flow.

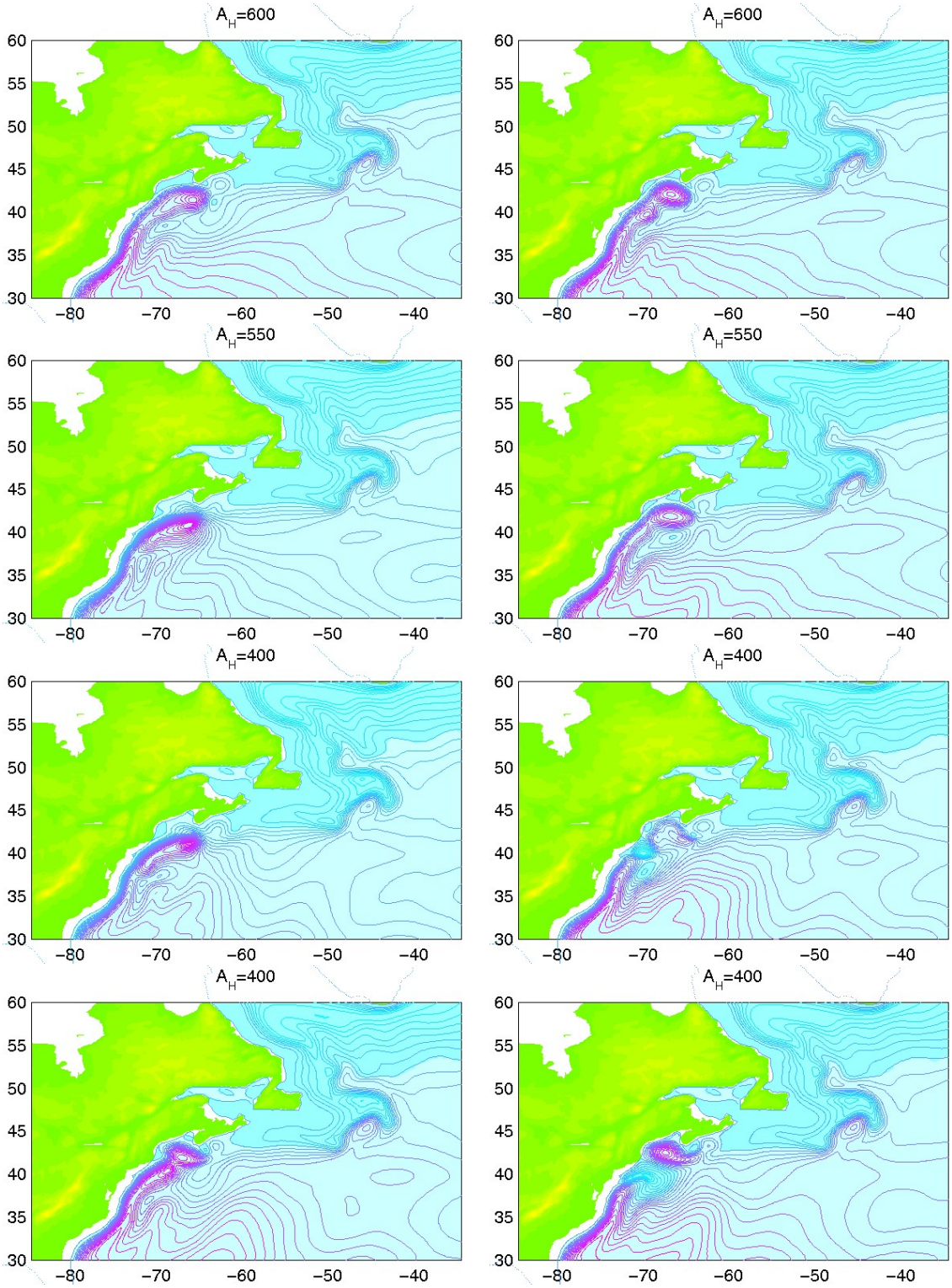
A_H=600
A_H=600
A_H=550
A_H=550
A_H=400
A_H=400
A_H=400
A_H=400
60
55
50
45
40
35
30
−80
−70
−60
−50
−40

Figure 5:

## 5 Proper orthogonal decomposition (POD) technique

The focus of this section is to obtain a reduced equivalent system of equations (26)-(27) to do the bifurcation analysis of the solution as the eddy viscosity parameter changes. A method to calculate such a system is the so called POD technique which generates a finite dimensional orthogonal basis that is optimal (in a sense to be defined bellow). A description of this technique is as follows.

*POD algorithm*

Let us consider the dynamical system

$$\frac{du}{dt} = F(t, u; \nu_h),\ u(0) = u_0,\ \ u(t) \in H,\ \ t \in (0, T] \tag{40}$$

where $H$ is a finite dimensional Hilbert space with scalar product $(\cdot, \cdot)$ and norm $\| \cdot \|$, and let us assume that we have a sequence $\{u^i\}_{1=1}^p$ of snapshots of $u(t)$. In the numerical computation the snapshots are the numerical solutions stored at predetermined time steps.

(1) Compute

$$\overline{u} = \frac{\sum_{i=1}^{p} \Delta\tau_{i-1} u^i}{\sum_{i=1}^{p} \Delta\tau_{i-1}},$$

where $\Delta\tau_{i-1} = \tau_i - \tau_{i-1}$ are the time instants at which the snapshots are stored. Then set

$$\widetilde{u}^i = u^i - \overline{u}^i.$$

(2) Compute the covariance matrix

$$K_{ij} = \sum_{i=1}^{p} \Delta\tau_{i-1} (\widetilde{u}^i, \widetilde{u}^j),\ \ 1 \leq i, j \leq p. \tag{41}$$

Notice that the matrix $K$ is symmetric and semi-definite positive.

(3) Calculate the eigenvalues $\{\lambda_k\}$ and eigenvectors $\{v_k\}$ of the matrix $K$ and order the basis $\{v_k\}$ after decreasing eigenvalues $\lambda_k$ (this $\{v_k\}$ will necesarily be orthogonal).

(4) Compute the orthonormal basis $\{\varphi_k\},\ \varphi_k \in H$, where

$$\varphi_k = \frac{\sum_{i=1}^{p} v_{ki} \widetilde{u}^i}{\| \sum_{i=1}^{p} v_{ki} \widetilde{u}^i \|} \tag{42}$$

Notice that this basis is optimal in the sense that minimizes the error in proyecting $\{u^i\}_{1=1}^{p}$ onto any n-dimensional space, for all $n$.

(5) *(Cut-off criterium)* The number $p^*$of energetically significant eigenvalues is given by the relation

$$\frac{\sum_{i=1}^{p^*}\lambda_i}{\sum_{i=1}^{p}\lambda_i} = \alpha \tag{43}$$

where $\alpha$ is a the cut-off parameter, $0 < \alpha \leq 1$. In our calculations we have taken $0.99 < \alpha < 1$.

(6) Approximate $u(t) \in H$ as

$$U(t) = \overline{u} + \sum_{i=1}^{p} a_i(t)\varphi_i \tag{44}$$

and determine the coefficients $a_i(t)$ by substitution of $U(t)$ in (40) and do a Galerkin projection on the span$\{\varphi_i\}_{i=1}^{p^*}$. Hence,

$$\frac{da_i(t)}{dt} = (F(t, U; \nu_h), \varphi_i), \quad a_i(0) = (U(0), \varphi_i). \tag{45}$$

To create the reduced system dynamically equivalent to (26)-(27) we store velocity snapshots of all the steady states plus snapshots of the periodic states corresponding to the values of $\nu_h = 670m^2s^{-1}$, $650m^2s^{-1}$ and $640m^2s^{-1}$. Table 1 shows the number of snapshots ($n_s$) and the number of the orthonormal basis functions ($n_b$) chosen in each state. The sum of these individual orthonormal functions generate the global orthonormal basis $\{\varphi_i\}_{i=1}^{30}$.

| $\nu_h$ | $n_s$ | $n_b$ |
|---|---|---|
| *steady states* | 10 | 10 |
| 670 | 26 | 6 |
| 650 | 200 | 9 |
| 640 | 24 | 5 |

Table 1

We approximate the semi-discrete solution $u_h(t)$ of (26)-(27) by an element $U(t)$ in the subspace $span\{\varphi_i\}_{i=1}^{30}$. Then, the substitution of $U(t)$ in (26)-(27) followed by a

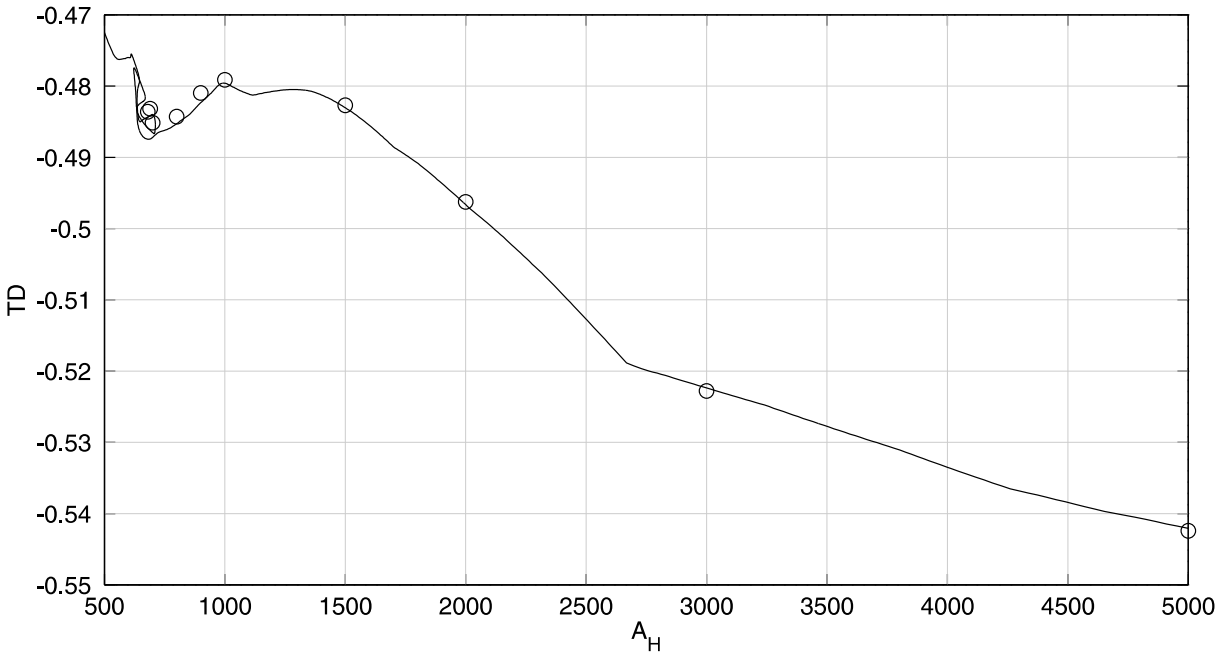


Figure 6: circle: semi-Lagrangian results; line: AUTO97 results

Galerkin projection onto $span\{\varphi_i\}_{i=1}^{30}$ gives the set of differential equations to determine the coefficients $a_i(t)$:

$$a_k'(t) = \sum_{i,j=1}^{30} d_{ijk} a_i(t) a_j(t) + \sum_{i=1}^{30} \left(q_{ki} + \nu_H q_{ki}'\right) a_i(t) + \left(r_k + \nu_H r_k'\right) \quad \forall k = 1, 2, \ldots, 30 \quad (46)$$

where

$$\begin{aligned}
d_{ijk} &= -\left(H\varphi_i \cdot \nabla\varphi_j, \varphi_k\right)_{L^2(\Omega)^2} \\
q_{ki} &= -\left(H\overline{u} \cdot \nabla\varphi_i, \varphi_k\right)_{L^2(\Omega)^2} - \left(H\varphi_i \cdot \nabla\overline{u}, \varphi_k\right)_{L^2(\Omega)^2} - \left(Hf\varphi_i^{\perp}, \varphi_k\right)_{L^2(\Omega)^2} - \gamma\delta_{ik} \\
q_{ki}' &= \left(H\nabla\varphi_i, \nabla\varphi_k\right)_{L^2(\Omega)^2} \\
r_{ki} &= -\left(H\overline{u} \cdot \nabla\overline{u}, \varphi_k\right)_{L^2(\Omega)^2} - \left(Hf\overline{u}, \varphi_k\right)_{L^2(\Omega)^2} - \gamma\left(H\overline{u}, \varphi_k\right)_{L^2(\Omega)^2} + \left(H\tau, \varphi_k\right)_{L^2(\Omega)^2} \\
r_{ki}' &= \left(H\nabla\overline{u}, \nabla\phi_k\right)_{L^2(\Omega)^2}
\end{aligned}$$

We use the program AUTO97 to compute the solutions of the equations (46) and the bifurcation diagram as $\nu_h$ varies. Figure 6 shows the bifurcation diagram and Figure 7 is a detail of bifurcation branches after the first Hopf bifurcation. As we see in Figure 6, the POD technique is able to capture well the steady state, but the prediction of the periodic, quasi-periodic and aperiodic states is not that good as Figure 7 shows, where blue region is for unstable periodic states and green region for stable ones.

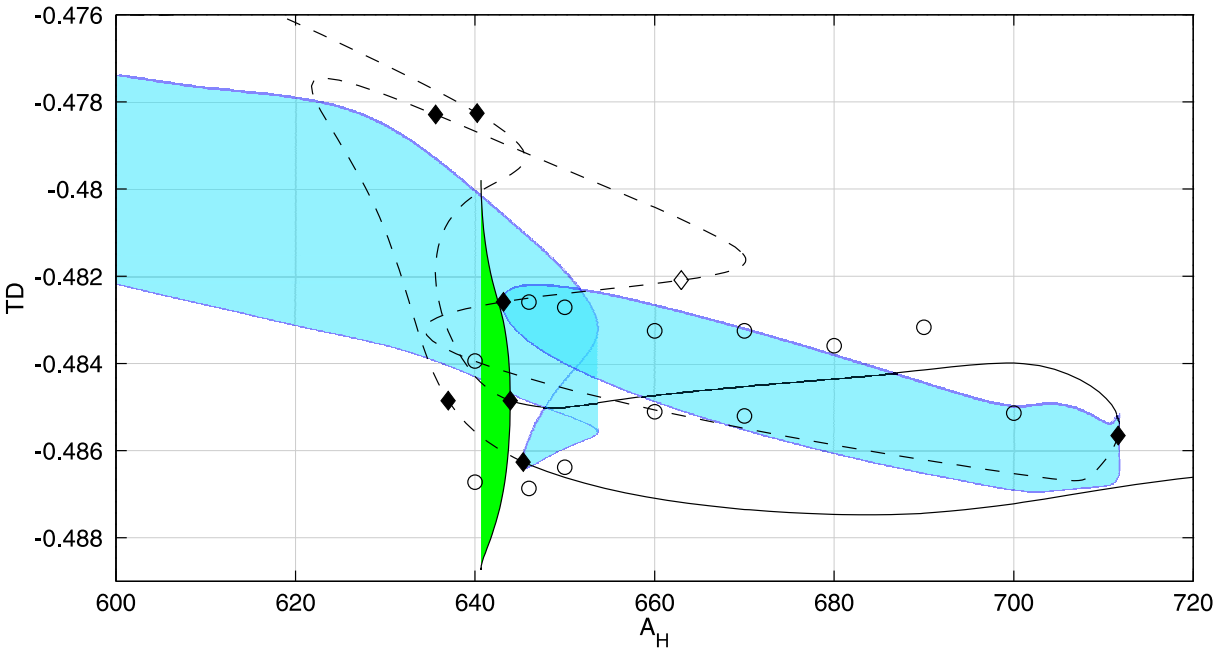


Figure 7: circle: semi-Lagrangian results; line: AUTO97 results; rhomboids: Hopf bifurcation (AUTO97)

## REFERENCES

[1] A. Allievi and R. Bermejo. Finite element modified method of characteristic for the Navier-Stokes equations. *Int. J. Numer. Method Fluids*, **32**, 439–464, 2000.

[2] P.S. Berloff and S.P. Meacham. The dynamics of an equivalent-barotropic model of the wind-driven circulation. *J. Mar. Res.*, **55**, 407–451, 1997.

[3] R. Bermejo. Analysis of a class of quasi-monotone and conservative semi-Lagrangian advection schemes. *Numer.Math.*, **87**, 597–623, 2001.

[4] R. Bermejo and A. Staniforth. The conversion of semi-Lagrangian advection schemes to quasi-monotone schemes. *Mon. Wea. Rev.*, **120**, 2622–2632, 1992.

[5] K. Bryan. A numerical investigation of a nonlinear model of a wind-driven ocean. *J. Atmos. Sci.*, **20**, 594–606, 1963.

[6] K.I. Chang, M. Ghil, K. Ide and C.C.A. Lai. Transition to aperiodic variability in a wind-driven double-gyre circulation model. *J. Phys. Oceanogr.*, **31**, 1260–1286, 2001.

[7] E.J. Doedel, A.R. Champneys, T.F. Fairgrieve, Y.A. Kuznetsov, B. Sandstede and X.J. Wang. AUTO97: Continuation and bifurcation software for ordinary differen-

tial equations. Department of Computer Science, Concordia University, Montreal, Canada, 1997.

[8] J. Doublas and T.F. Russell. Numerical methods for convection-dominated diffusion problems based on combining the method of the characteristics with finite elements or finite differences. *SIAM J. Numer. Anal.*, **9**, 871–883, 1982.

[9] P. Galán del Sastre. *Cálculo numérico del atractor en ecuaciones de Navier-Stokes aplicadas a la circulación del océano*. Doctoral Dissertation, Universidad Complutense de Madrid, Departamento de Matemática Aplicada, 2004.

[10] J.L. Guermond and L. Quartapelle. On the approximation of the unsteady Navier-Stokes equations by finite element projection methods. *Numer.Math.*, **80**, 207–238, 1998.

[11] J.L. Guermond. Un résultat de convergence d'ordre deux en temps pour l'approximation des équations de Navier-Stokes par une technique de projection incrémentale. *M2AN Math. Model. Numer. Anal.*, **33**, 169–189, 1999.

[12] E. Hairer, S.P. Nørsett and G. Wanner. *Solving Ordinary Differential Equations I. Nonstiff Problems*. Springer-Verlag, 1987.

[13] S. Jiang, F.F. Jin and M.Ghil. Multiple equilibria, periodic, and aperiodic solutions in a wind-driven, double-gyre, shallow-water model. *J. Phys. Oceanogr.*, **25**, 764–786, 1995.

[14] J.L. Lions, R. Temam and S. Wang. On mathematical problems for the primitive equations of the ocean: the mesoscale midlatitude case. *Nonlinear Anal.*, **40**, 439–482, 2000.

[15] W. Munk. On the wind-driven ocean circulation. *J. Meteorol.*, **7**, 79–93, 1950.

[16] W. Munk and G.F. Carrier. The wind-driven circulation in ocean basins of various shapes. *Tellus*, **2**, 158–167, 1950.

[17] J. Pedlosky. *Geophysical Fluid Dynamics*. Springer-Verlag, 1987.

[18] O. Pironneau. On the transport-diffusion algorithm and its applications to the Navier-Stokes equations. *Numer.Math.*, **38**, 309–332, 1982.

[19] R. Temam. *Navier-Stokes equations. Theory and numerical analysis*. North-Holland Publishing Co., 1977. Studies in Mathematics and its Applications, Vol. 2.

[20] G. Veronis. Wind-driven ocean circulation. Part 1. *Deep-Sea Res.*, **13**, 17–29, 1966.